Genetic-Algorithm-Based Design for Rideshare and Heterogeneous Constellations

Katherine M. Wagner* and Jonathan T. Black†
Virginia Polytechnic Institute and State University, Blacksburg, Virginia 24061

https://doi.org/10.2514/1.A34527

Responsive and resilient space-based systems are needed to satisfy changing mission requirements and react to unforeseen challenges. Nontraditional constellations, such as heterogeneous and rideshare constellations, have the potential to increase resiliency and responsiveness, as can using commercial off-the-shelf parts. However, these constellation types introduce design challenges that cannot be solved by analytical techniques. A novel methodology for optimizing these constellations using a multi-objective genetic algorithm and model-based systems engineering techniques is introduced. Included in this methodology are new techniques for measuring constellation resiliency and rapidly determining reachability between two orbits. The methodology is applied to a validation case of designing a Mars-orbiting position, navigation, timing, and communications constellation. The methodology is then used to examine the viability of using rideshare opportunities to construct a satellite constellation. The constellation must provide regional imaging coverage in the event of a natural disaster, and its efficacy is evaluated both in the nominal case and in the case when multiple satellites have failed.

I. Introduction

THE satellite constellation design paradigm has seen increased use of smaller, less costly satellites within the past decade [1]. Between 2012 and 2017, the number of small satellites (less than 600 kg) launched per year increased sixfold, whereas more massive satellites were launched at a nearly constant rate over the same time period [2]. This shift is driven by many factors, including miniaturization of satellite components, standardization and the availability of commercial off-the-shelf (COTS) components, and disaggregation of satellite missions and components across multiple platforms [1,3–5]. New tools and methodologies are needed to accommodate the unique challenges and capabilities of these nontraditional systems. The Disaggregated Integral Systems Concept Optimization Technology (DISCO-Tech) methodology was created to address these challenges, including modeling disaggregated constellations, optimizing satellite payloads across multiple buses, analyzing mission performance of degraded constellations, and leveraging nontraditional launch opportunities.

The DISCO-Tech methodology is overviewed herein. Particular focus is given to the development of new techniques for determining reachability between two orbits given constraints on propellant and thrust and for quantifying the resiliency of a proposed satellite constellation based on the constellation's ability to perform in the event of asset loss or failure. The DISCO-Tech methodology is then applied to the problem of designing a Mars-orbiting communications and position, navigation, and timing constellation. This first scenario is meant to serve as a validation case and is therefore restricted to a single objective function and a fixed set of potential architectures. It demonstrates the ability of DISCO-Tech to compare heterogeneous and homogeneous constellations. A second scenario requiring the design of a constellation of imaging satellites providing coverage of the State of California for the purposes of fire detection is also considered. The constellation is manifested using rideshare opportunities, then onboard propellant is used to modify the orbits after launch. The satellites use only COTS components designed for nanosatellites. This scenario demonstrates DISCO-Tech's ability to leverage nontraditional launch opportunities, optimize dynamic constellations that undergo reconfiguration, and measure degraded constellation performance.

II. Background

Spacecraft can fail for a variety of reasons, including launch failures, radiation, thermal stresses, and electronics failures [6]. Because the failure of even a single satellite detracts from a constellation's ability to perform its mission, it is beneficial to explore architectures that are resilient to failure and to quantify the effect of a failure on mission performance.

Disaggregation is one method of increasing the resilience of space systems [7]. As identified by the Air Force Space Command, the disaggregation strategies of interest are as follows [8]:

1) Fractionation: the dispersion of a system into multiple on-orbit modules, where the subsystems interact wirelessly

2) Functional disaggregation: the dispersion of payloads or sensors onto separate satellite platforms

3) Hosted payload disaggregation: the dispersion of payloads as secondary payloads onto other satellite systems

4) Multi-orbit disaggregation: the use of satellites in multiple orbital planes that work together to perform a mission

5) Multidomain disaggregation: the use of assets in multiple domains that work together to perform a mission

Disaggregation has previously been applied to problems of space-based weather monitoring and fire detection [9–12]. Multidomain disaggregation in particular has been used to design space situational awareness architecture, though the study lacked the dynamic architecture design capabilities provided by DISCO-Tech [13].

By decreasing system complexity, fractionation and functional disaggregation can often employ smaller spacecraft due to decreased power and data throughput requirements. Multi-orbit disaggregation can also indirectly decrease satellite size, as a multi-orbit constellation in low Earth orbit (LEO) may use smaller, less powerful payloads to provide coverage similar to a single large satellite at a higher altitude. Small satellites benefit from lower costs and opportunities for standardization not available for large satellites. However, they come with their own set of challenges. For example, the small-form-factor, low-cost satellites known as CubeSats are particularly susceptible to failure due to their use of COTS parts, low budgets, and high risk tolerance. A 2017 study by the Aerospace Corporation found that academic CubeSat missions failed 55% of the time, whereas

Presented in two parts at the AAS/AIAA Astrodynamics Conference in Stevenson, WA, on August 20–24, 2017 (Paper AAS 17-813), and the AAS/AIAA Space Flight Mechanics Meeting in Ka'anapali, HI, on January 13–17, 2019 (Paper AAS 19-402); received 11 April 2019; revision received 20 March 2020; accepted for publication 24 April 2020; published online 26 June 2020.

*Graduate Student, Crofton Department of Aerospace and Ocean Engineering. Member AIAA.

†Professor, Crofton Department of Aerospace and Ocean Engineering. Associate Fellow AIAA.

commercial CubeSat endeavors failed 23% of the time [14]. Despite their failure rate, CubeSat constellations can enable critical space missions by providing rapid response through their rapid development times. Additionally, their small size allows them to be launched as secondary payloads when their mission has some flexibility in the required orbital configuration. CubeSats can therefore play an important role in a disaggregated constellation if their limitations are controlled.

As part of these considerations, the effect of the failure of one or more satellites on the ability of the constellation to perform its mission must be assessed. Previous work has measured constellation resilience based on the predicted failure rate [15] and the predicted number of satellites on orbit [16]. Stenger performed network analysis for a degraded Iridium constellation, selecting the worst-case removals in batches of 12 by finding the satellites that appeared most often in the packet paths and removing them [17]. However, this method is not mathematically rigorous for nonuniform constellations because the problem of satellite access cannot be solved recursively. To illustrate, a case in which satellites are spaced unevenly in an orbital plane is shown in Fig. 1. The satellites are assumed to be placed in an equatorial orbit, with ground stations also on the equator. In the nominal case, the largest gap occurs between satellites C and D. If a single failure occurs (the 1-removal case), the satellite whose removal would result in the largest gap is satellite C, denoted by an orange triangle. If the 2-removal case continues from the 1-removal case by assuming that C has already been removed, the next most damaging satellite to remove is B. However, considering the 2-removal problem independently from the 1-removal problem shows that the best two satellites to remove are D and E, denoted by red squares, as removing these two satellites creates the largest gap in true anomaly and therefore the largest gap in coverage. Therefore, relying on recursion to determine the worst-case removals yields an incorrect answer. It is therefore beneficial to develop a rigorous methodology for determining the satellites whose removal is most damaging to the constellation performance.

Another issue in the deployment of nanosatellite constellations is getting all of the assets into orbit. In traditional spacecraft constellations, the launch costs are a relatively small portion of the overall budget; an example scenario in Ref. [18] predicts a 14% launch cost. Nanosatellites, however, can be as cheap as a couple hundred thousand dollars [19]. Because launch vehicles cost tens to hundreds of millions of dollars, the use of dedicated launches for low-cost missions is infeasible unless hundreds of satellites can share a launch vehicle [20]. However, small satellites can be launched as secondary payloads via rideshare programs for about $30,000 per kilogram [19]. Additionally, academic groups may qualify for free launch services through the Educational Launch of Nanosatellite (ELaNa) missions [21]. The downside of constellations built using rideshare alone, sometimes called ad hoc constellations, is that the irregular distribution of satellites results in large gaps in coverage compared with a symmetric constellation like a Walker constellation. Previous studies have quantified these differences, but have shown that performance can be improved through optimization of the rideshare selection. One such study randomly selected combinations of satellites from previous launches to characterize the range of performance for ad hoc constellations providing global coverage [22]. Reference [23] used a multi-objective genetic algorithm to determine an optimal rideshare manifest for providing global coverage. A single solution from the resulting nondominated front was selected and its resiliency assessed after the optimization. Finally, a method was developed for optimally manifesting secondary payloads using linear programming techniques, but this method requires that the desired orbits for the satellites be known a priori [24].

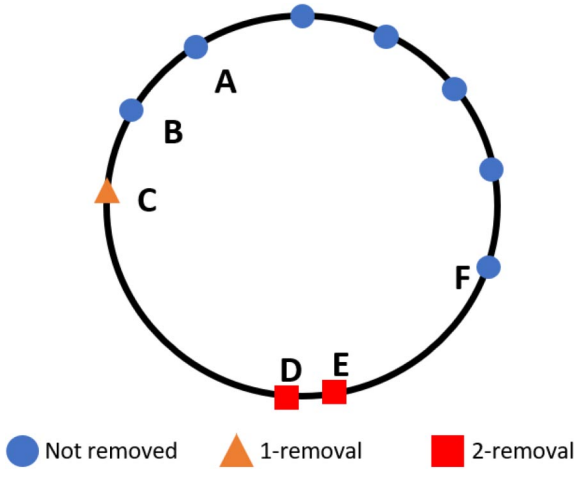

Fig. 1 Representative nonuniform satellite distribution.

III. Methodology

The DISCO-Tech methodology was used to formulate and solve both scenarios. The DISCO-Tech algorithm is modular, with each module performing a different task of the optimization. Core modules of the code are described in detail in Ref. [25]. Unchanged modules are briefly summarized below, whereas new or updated modules are described in detail.

A. Optimization

DISCO-Tech uses a modified version of the epsilon nondominated sorting genetic algorithm II (ϵ-NSGAII) to solve multi-objective optimization problems [26]. It combines the epsilon dominance feature of ϵ-NSGAII with the archive feature of the Borg genetic algorithm but maintains the use of generations to facilitate ease in parallelization [27]. It differs from Borg and ϵ-NSGAII in that it uses a variable-length crossover operation, as described in Ref. [25]. Evolutionary algorithms have successfully been applied to satellite constellation design problems in the past, making them suitable optimizers for this study [26,28–30].

B. Reachability

Literature on constellation reconfiguration has restricted analysis to specific sets of maneuvers. One study restricted reconfiguration to in-plane maneuvers, and then used a genetic algorithm to solve for the two-burn transfers yielding the best coverage in the final configuration [26]. Other studies restrict the initial and final constellations to known sets of orbits, presolving for the propellant needed to go between each combination of orbits and then solving the assignment problem to find the optimal set of transfers [31–33].

A general framework was desired to rapidly determine the reachability of one orbit from another. Although methods exist for generating the reachable set [34–37], they rely on numerical simulation and are too computationally expensive to call for each solution during the optimization because the reachable set will change as the initial orbit changes. Instead, an estimation of the propellant used is generated using a linearized version of Gauss's variational equations (GVEs). If the estimated propellant is less than or equal to the available propellant, the final orbit is considered to be reachable from the initial orbit. This section outlines the linearization and examines the regions for which the linearization is within some user-defined bounds of the nonlinear system.

Previous research linearized GVEs about the final orbit and used the resulting equations with model predictive control (MPC) to calculate the required controls to maneuver from one orbit to another [38]. This linearization serves as the basis for DISCO-Tech's approach, though the MPC process was deemed unnecessarily costly because the total propellant expenditure is needed, not the entire control history. Furthermore, the linearization presented in Ref. [38] is improved through the use of the modified equinoctial orbital elements (MEOEs), by treating the true longitude as an independent parameter, and by improved analysis of the validity of the linearization. It is assumed that the final value of the true longitude is irrelevant, as it can be set afterward by temporarily raising or lowering the orbit using a comparatively small amount of propellant or by holding the satellite at an intermediate stage in its transfer until the desired phasing has been reached. It is also assumed that the maximum acceleration of

the spacecraft does not change over time despite the change in the spacecraft's mass.

1. Derivation

GVEs are of the form

$$\frac{\mathrm{d}\boldsymbol{x}}{\mathrm{d}t} = \boldsymbol{f}(\boldsymbol{x}) + B(\boldsymbol{x})\boldsymbol{u} \tag{1}$$

where $\boldsymbol{x}$ is the vector of orbital elements and $\boldsymbol{u} = [u_r, u_\theta, u_h]^T$ are the control accelerations in the local-vertical–local-horizontal (LVLH) frame. This formulation uses the set of MEOEs, a set of nonsingular elements defined in Ref. [39,40]. The MEOEs are denoted by $\boldsymbol{x} = [p, f, g, h, k, L]^T$, where the true longitude L is the only rapidly changing variable. p is the semiparameter of the orbit. The remaining four elements lack physical meaning but are defined as $f = e\cos(\omega + \Omega)$, $g = e\sin(\omega + \Omega)$, $h = \tan(i/2)\cos(\Omega)$, and $k = \tan(i/2)\sin(\Omega)$, where e is the eccentricity, i is the inclination, ω is the argument of periapsis (AOP), and Ω is the right ascension of the ascending node (RAAN). $\boldsymbol{f}(\boldsymbol{x}) \in \mathbb{R}^6$ represents the dynamics of the elements in the absence of control, and $B(\boldsymbol{x}) \in \mathbb{R}^{6\times 3}$ is the input effect matrix. These matrices can be constructed from the equations in Ref. [39].

With the exception of true longitude, the orbital elements are constant in the absence of perturbations like oblateness effects. Form a reduced set of elements $z = [p, f, g, h, k]^T$. Equation (1) can be rewritten as

$$\frac{\mathrm{d}}{\mathrm{d}t}\begin{bmatrix} z \\ L \end{bmatrix} = \boldsymbol{f}(z, L) + B(z, L)\boldsymbol{u} \tag{2}$$

Because the first five elements of $f(x)$ are zero for the two-body problem, the dynamics of these elements can be written as

$$\frac{\mathrm{d}z}{\mathrm{d}t} = \overline{B}(z, L)\boldsymbol{u} \tag{3}$$

where $\overline{B}(z, L)$ is the first five rows of $B(z, L)$. The equation is affine in $\boldsymbol{u}$ but nonlinear in z due to the dependence of $\overline{B}$ on z.

It is advantageous to treat the true longitude L as an independent parameter, so the conditions under which such an assumption holds are examined. The dynamics of L are described by

$$\frac{\mathrm{d}L}{\mathrm{d}t} = \sqrt{\frac{\mu}{p^3}}(1 + e\cos(\theta))^2 + \sqrt{\frac{p}{\mu}}\frac{\tan(i/2)\sin(\theta + \omega)}{1 + e\cos(\theta)}u_h \tag{4}$$

The classical orbital elements are used to provide a sense of physical understanding, with θ being the true anomaly. The control input has the greatest influence on the dynamics of L when the second term of the previous equation is maximized. R is defined as the ratio between the second term in Eq. (4) and the first term in Eq. (4). R is maximized if $\sin(\theta + \omega) = 1$, $\cos(\theta) = -1$, and u_h is equal to its maximum possible acceleration $u_{\max}$:

$$R_{\max} = \frac{u_{\max}a^2(1 - e^2)^2\tan(i/2)}{\mu(1 - e)^3} \tag{5}$$

This ratio quantifies the maximum relative impact that the control thrust can have on the dynamics of L. By setting an upper limit on the instantaneous value of the ratio, a maximum allowable thrust acceleration for various combinations of a, i, and e can be calculated. Equation (5) is zero for an inclination of zero because thrusting in the angular momentum direction at this inclination will not affect the true longitude. Figure 2 shows the maximum allowable thrust acceleration such that the ratio $R_{\max}$ at apoapsis will not exceed 0.1. When the control accelerations are smaller than those described in the plot for a given combination of semimajor axis, eccentricity, and inclination, the impact of the control on the growth of the true longitude can be ignored.

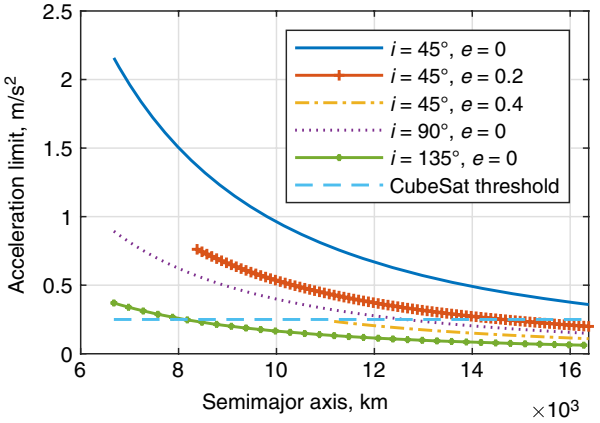

Fig. 2 Thrust acceleration limit for orbits at various inclinations and eccentricities.

Nanosatellites tend to employ micropropulsion systems with low thrusts on the order of millinewtons [41]. The control influence on L can be safely ignored for these cases. High-thrust CubeSat propulsion systems with up to 1.25 N of thrust are in development.[‡] Assuming that these systems would be used exclusively with larger CubeSats with a dry mass of at least 5 kg, the corresponding acceleration would be at most 0.25 m/s^2. From Fig. 2, it can be seen that satellites in LEO with eccentricity less than 0.4 and inclinations less than 135° will satisfy this constraint. If a nanosatellite is constrained to LEO, either due to rideshare availability or due to sensor requirements, the assumption that the control does not significantly affect the true longitude will hold. The rate of change of L is then $\mathrm{d}L/\mathrm{d}t = \sqrt{\mu}q^2p^{-3/2}$. The values of L can be approximated either by holding the MEOE fixed at either the initial or final values or by linearly interpolating between the initial and final values and calculating the growth of L at each time step. The approximation of the secular growth rate distorts the relationship between time steps and steps of L, but the validation cases tested in Sec. III.B.1 demonstrate that the effect does not significantly impact the results. The effect can be mitigated by using smaller time steps or by iterating through the problem multiple times, using the previous solution to generate the approximation of L. The initial formulation linearly interpolates values of a and e between the initial and final values over the analysis period and then uses those values to calculate the true longitude. Using this process, true longitude can be treated as a function of time alone, allowing it to be treated as an independent parameter in the linear program (LP) if the control thrusts are within the bounds specified in Fig. 2. Equation (3) can then be rewritten as $\mathrm{d}z/\mathrm{d}t = \overline{B}(z, L(t))\boldsymbol{u}$.

Performing a Taylor series expansion of Eq. (3) about some reference orbit z_s gives

$$\frac{\mathrm{d}z}{\mathrm{d}t} = \left(\overline{B}(z_s, L(t)) + \left.\frac{\partial\overline{B}}{\partial z}\right|_{z=z_s}\Delta z\right)\boldsymbol{u} + \mathrm{HOT} \tag{6}$$

where $\Delta z = z - z_s$. $\partial\overline{B}/\partial z$ in the second term is a tensor of rank three. The higher-order terms (HOT) are neglected. The equation for a single element z_i is given below for clarity, with b_{ij} being the element of B in the ith row and the jth column.

$$\frac{\mathrm{d}z_i}{\mathrm{d}t} \approx [b_{i1}b_{i2}b_{i3}]\boldsymbol{u} + \left.\begin{bmatrix}\Delta p\\ \Delta f\\ \Delta g\\ \Delta h\\ \Delta k\end{bmatrix}^T\begin{bmatrix}\partial b_{i1}/\partial p & \partial b_{i2}/\partial p & \partial b_{i3}/\partial p\\ \partial b_{i1}/\partial f & \partial b_{i2}/\partial f & \partial b_{i3}/\partial f\\ \partial b_{i1}/\partial g & \partial b_{i2}/\partial g & \partial b_{i3}/\partial g\\ \partial b_{i1}/\partial h & \partial b_{i2}/\partial h & \partial b_{i3}/\partial h\\ \partial b_{i1}/\partial k & \partial b_{i2}/\partial k & \partial b_{i3}/\partial k\end{bmatrix}\right|_{z=z_s}\boldsymbol{u} \tag{7}$$

[‡]http://www.rocket.com/files/aerojet/documents/CubeSat/MPS-130%20data%20sheet%20crop.pdf.

$$\approx(\boldsymbol{b}_i + (J_i\Delta z)^T)\boldsymbol{u} \tag{8}$$

The second term results in a nonlinear equation because the term contains a product of Δz and $\boldsymbol{u}$. The system can be solved using linear programming techniques if the nonlinear term can be neglected. This simplification is valid if the magnitudes of the derivatives of $\overline{B}$ are small compared with the values of $\overline{B}$ itself. The ranges over which this assumption is valid are examined.

To determine the allowable extent of the nonlinearity due to a variation in one of the MEOEs, a bound is set on the ratio of the magnitudes of the nonlinear and linear terms causing a change in element i due to the difference in element j from the stationary orbit:

$$Q_{ij} = \frac{|\Delta z_j|\|\boldsymbol{j}_{ij}\|}{\|\boldsymbol{b}_i\|} = \frac{|\Delta z_j|\sqrt{(\partial b_{i1}/\partial z_j)^2 + (\partial b_{i2}/\partial z_j)^2 + (\partial b_{i3}/\partial z_j)^2}}{\sqrt{b_{i1}^2 + b_{i2}^2 + b_{i3}^2}} \tag{9}$$

$\boldsymbol{j}_{ij}$ is the jth column of the J_i matrix. By setting an upper limit on the value of Q_{ij}, $Q_{\max}$, bounds on each of the orbital elements can be developed. Since the bounds on Δz_j must satisfy the imposed limits on $Q_{ij}\ \forall\ i \in [1,5]$, the smallest value of Δz_j calculated by the five equations is selected by taking the minimum over i. This limit should be satisfied for all values of L. However, some elements of $\overline{B}$, such as b_{21}, go to zero at certain values of L. As a result, the ratio near these points is poorly defined. Furthermore, a large Q_{ij} value occurring when $\boldsymbol{b}_i$ is small still results in a small magnitude change in $\boldsymbol{b}_i$. To avoid these singularities, the denominator used in Eq. (9) is not the instantaneous value for a given L but the average value calculated by averaging $\|\boldsymbol{b}_i\|$ over L. This average value is denoted as $\|\boldsymbol{b}_i\|_{\text{avg}}$. Because all terms in the numerator of Eq. (9) are a function of L, take the minimum of $|\Delta z_j|$ over L to ensure the most conservative bounds. Mathematically, this relationship can be written by inverting Eq. (9) to obtain

$$|\Delta z_j| \le \min_{i\in[1,5]}\left(\min_{L\in[0,2\pi]}\left(Q_{\max}\frac{\|\boldsymbol{b}_i\|_{\text{avg}}}{\|\boldsymbol{j}_{ij}(L)\|}\right)\right) \tag{10}$$

Using the process described above, bounds on the linearization are generated for an orbit with nominal values of $a = 7000$ km, $e = 0.1$, $i = \pi/4$, $\Omega = \pi/6$, and $\omega = \pi/12$ and $Q_{\max} = 0.1$. To determine the impact of the initial value of each orbital element on the bounds, the initial orbital elements are varied one at a time while holding the others fixed. a is varied from 6678 to 16,378 km, e is varied from 0 to 0.8, i is varied from 0 to 180°, Ω is varied from 0 to 360°, and ω is varied from 0 to 360°. Figure 3 shows the results for the combinations of orbital parameters having the most significant impacts.

The main determining factor in the semimajor axis bounds is itself, with larger semimajor axes having larger bounds. For a LEO, a limit of $|\Delta a| = 500$ km ensures that the bounds on the linearization are satisfied, as is shown in Fig. 3a. These bounds consider only the GVE linearization and do not account for drag or other nonlinearities. Figure 3b shows that eccentricity is the main determining factor for its own bounds, with larger eccentricity having smaller bounds. Inclination influences the bounds on eccentricity as well, as shown in Fig. 3c. For an orbit with low eccentricity, bounds of about 0.1 are acceptable. As shown in Fig. 3d, the inclination bounds decrease with increasing inclination. A high-thrust CubeSat propulsion system may provide approximately $\Delta v = 570$ m/s for a 5 kg satellite. The achievable inclination change with $\Delta v = 570$ m/s at an altitude of 1000 km is only 4.4°. This high propellant requirement, coupled with the large bounds on inclination, makes it unlikely that a satellite would maneuver more than a couple of degrees in inclination, rendering the linearization valid for all practical cases barring a retrograde orbit with inclination greater than 120°.

Overall, the linearization will hold when the semimajor axis error is kept below 500 km, the eccentricity error kept below 0.1 for low eccentricities and below 0.05 for eccentricities near 0.5,

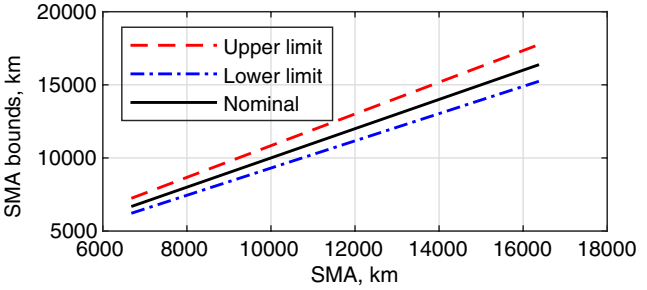

a) Semimajor axis (SMA) bounds with increasing SMA

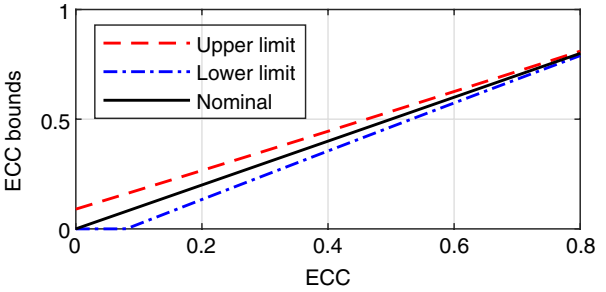

b) Eccentricity (ECC) bounds with increasing ECC

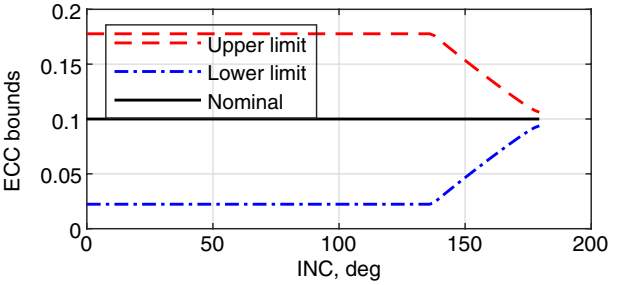

c) Eccentricity (ECC) bounds with increasing inclination (INC)

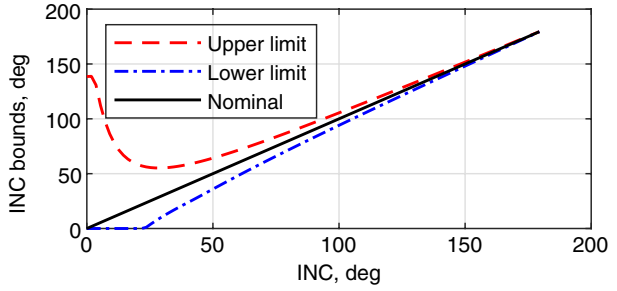

d) Inclination (INC) bounds with increasing INC

Fig. 3 Element limits for valid linearization under changing initial element values.

the eccentricity kept below 0.5, the inclination kept below 120°, changes in AOP kept below 50°, and changes in RAAN and inclination kept below 10° for prograde orbits and 5° for retrograde orbits.

Now that it has been shown that the nonlinear term in Eq. (6) can be neglected in the cases described above, the linear equation

$$\frac{\mathrm{d}z}{\mathrm{d}t} = \overline{B}(z_s, L(t))\boldsymbol{u} \tag{11}$$

can be used to approximate the change in the orbital elements over time for cases satisfying the bounds on thrust and orbital element error described previously. As an initial guess, the reference orbit is a linear interpolation between the initial and final orbits. Fidelity can be improved by performing multiple iterations, using the solution from the previous iteration as the reference orbit for the next.

Applying the variation of constants formula to the above equation gives

$$z(t) = z_0 + \int_{t_0}^{t}\overline{B}(z_s, L(v))\boldsymbol{u}(v)\,\mathrm{d}v \tag{12}$$

If the system is discretized by setting $t = k\Delta t$, using it to calculate $L_k = L(k\Delta t)$, and treating $\overline{B}$ and $\boldsymbol{u}$ as being fixed at each time step, the equation becomes

$$z_{k+1} = z_0 + \Delta t \sum_{j=0}^{k} \overline{B}_j \boldsymbol{u}_j \tag{13}$$

With Eq. (13), the problem of finding a propellant-optimal trajectory between the initial and final orbits can now be formulated as a LP. If the three control thrusts are provided independently using three separate thrusters, the total Δv required for the maneuver is $\Delta v = \sum_k (|u_{rk}| + |u_{\theta k}| + |u_{hk}|)\Delta t$. However, in the case where a single thruster is providing control, the required Δv is $\Delta v = \sum_k \sqrt{u_{rk}^2 + u_{\theta k}^2 + u_{hk}^2}\Delta t$. Even in the latter case, the simplifying assumption is made to use the former value for Δv. To treat the absolute values in the Δv formulation, it is necessary to create separate variables u_{ik}^+ and u_{ik}^-, both in $[0, u_{\max}]$, such that $u_{ik} = u_{ik}^+ - u_{ik}^-$. The minimization will ensure that at most one of u_{ik}^+ and u_{ik}^- is nonzero. The LP formulation can be written as

$$\text{Minimize} \qquad \Delta t \sum_k \sum_i u_{ik}^+ + u_{ik}^-$$

with decision variables:

$$u_{ik}^+ \in [0, u_{\max}] \quad \forall\ k = 0, 1, \ldots, k_f, i \in \{r, \theta, h\}$$

$$u_{ik}^- \in [0, u_{\max}] \quad \forall\ k = 0, 1, \ldots, k_f, i \in \{r, \theta, h\}$$

such that:

$$z_{fd} - \zeta_f \le z_0 + \Delta f \sum_{j=0}^{k_f} \overline{B}_j \boldsymbol{u}_j \le z_{fd} + \zeta_f$$

where ζ_f is the allowable error in the final state, and the desired final state is z_{fd}. Similar LP formulations have been used for trajectory optimization using the Hill–Clohessy–Wiltshire equations or the Gim–Alfriend equations as a basis, such as in Ref. [42]. Because the control is held constant during each step, reaching an exact state may be impossible, requiring the inclusion of error bounds. Open source or commercial LP solvers can be used to obtain the optimal trajectory. Once the optimal solution is known, the orbital elements at each step k can be calculated using Eq. (13). The approximate Δv required is equal to the objective function value.

This formulation does not consider uncertainties in position and velocity or pointing accuracy. For Earth-based systems with low-cost GPS receivers, position and velocity errors are 10 m and 25 cm/s, respectively.[§] These errors are small compared with the magnitude of the position and velocity vectors and therefore have negligible impact on the orbital elements. A satellite with a pointing accuracy of 1° would experience less than a 2% change in the thrust vector from its nominal value.[¶] Techniques for handling state errors in satellite maneuvering include Kalman filtering [43], MPC [42], and the Lyapunov direct stability theorem [44]. Similar measures could be adapted at the cost of increased computational complexity.

2. *Validation*

Two scenarios are used to test the problem formulation. First, the problem of raising a circular orbit from 1000 km in altitude to 1500 km in altitude using a maximum acceleration of 0.01 m/s^2 is considered. According to Ref. [45], the optimal low-thrust orbit raise for a circular orbit is a continuous thrust in the velocity vector direction and consumes a total Δv of $\Delta v = |\sqrt{\mu/a_0} - \sqrt{\mu/a_f}|$. The time needed to complete the maneuver is $t_f - t_0 = (\mu/u_{\max})|a_0^{-1/2} - a_f^{-1/2}|$. For the given problem, the required Δv according to the equation is 237.1 m/s.

The scenario was permitted to run for 1.05 times the predicted time needed to complete the maneuver. The semimajor axis was assumed to vary linearly between the initial and final values, with these interpolated values being used in the B_k matrices at each time step. The estimated velocity required for the orbit raise is 235.9 m/s, resulting in a deviation from the analytical solution of less than 1%.

The second scenario requires an inclination change of 2° within 40 orbital periods. The orbit is circular and has an altitude of 1000 km. From GVEs, changes in inclination are caused by thrusting in the angular momentum direction, $\mathrm{d}i/\mathrm{d}t = ru_h \cos(\omega + \theta)/h$ [46]. Because of the cosine term, the impact from u_h is maximized at the ascending and descending nodes. Near the nodes, thrust in the angular momentum has little impact on other orbital elements, so the impact on i can be considered independently. If thrusting is performed for some time period ΔT centered on the nodal crossing with a constant acceleration u_c, the change in inclination for a single maneuver for a circular orbit can be shown to be

$$\delta i = \frac{2u_c a^2 \sin(n\Delta T/2)}{\mu\sqrt{1 - e^2}} \tag{14}$$

where n is the mean motion. Because 40 orbital periods are allowed for the inclination to occur, there are 80 nodal crossings and therefore 80 propulsion events, each resulting in an inclination change of 0.025°. If u_c is 0.01 m/s^2, the time for each maneuver ΔT can be obtained from Eq. (14) and is equal to 322 s. The total Δv for all 80 maneuvers is therefore equal to 257.7 m/s. The linear programming approach predicted a Δv of 253.9 m/s, yielding an error of 1%. These examples, when combined with the mathematical validation provided above, bound the accuracy of the linearization approach in predicting the Δv required for a LEO transfer. The predicted Δv can then be used to determine the reachability of one orbit from another.

C. Coverage

Because the calculation of satellite revisit metrics is nonlinear and computationally expensive, the rise and set times are computed for the nominal constellation, the satellite constellation from which no assets have been removed. The method used for calculating the rise and set times is adapted from the methods developed by Alfano [47]. Alfano uses a coarse time step to find the satellite positions over time, and then uses quintic interpolation to approximate the rise–set times of the satellites between the steps of the propagation. Alfano developed equations describing constraints on the maximum range, minimum and maximum elevation angles, and minimum and maximum azimuthal angles. For the purposes of this work, only the maximum range and minimum elevation equations are used:

$$f_R(t) = R(t) - R_{\text{LIM}} \tag{15}$$

$$f_\phi(t) = \left(\cos^{-1}\left\{\frac{\cos[\phi(t)]}{R(t)}\right\} - \phi(t)\right) - \left\{\cos^{-1}\left[\frac{\cos(\phi_{\text{LIM}})}{R(t)}\right] - \phi_{\text{LIM}}\right\} \tag{16}$$

where $R(t)$ is the range from a satellite to a ground station at time t, $\phi(t)$ is the elevation angle from the ground station to the satellite, R_{LIM} is the maximum allowable range, and ϕ_{LIM} is the minimum allowable elevation angle. Additionally, an equation for a constraint on the maximum off-boresight angle of the ground station with respect to the satellite is developed. The off-boresight angle $\theta(t)$ can be calculated as

$$\theta(t) = \cos^{-1}\left[\frac{\boldsymbol{R}(t) \cdot \boldsymbol{p}(t)}{\|\boldsymbol{R}(t)\|}\right] \tag{17}$$

where $\boldsymbol{R}(t)$ is the vector from the satellite to the ground station and $\boldsymbol{p}(t)$ is the unit vector in the direction of the boresight axis of the sensor.

For the off-boresight angle constraint, the equation is a slight modification of Eq. (16):

[§]https://www.cubesatshop.com/product/nss-gps-receiver/.

[¶]https://www.bluecanyontech.com/static/datasheet/BCT_DataSheet_Components_StarTrackers.pdf.

$$f_\theta(t) = \left(\cos^{-1}\left\{\frac{\cos[\theta(t)]}{R(t)}\right\} - \theta(t)\right) - \left\{\cos^{-1}\left[\frac{\cos(\theta_{\text{LIM}})}{R(t)}\right] - \theta_{\text{LIM}}\right\} \tag{18}$$

where θ_{LIM} is the maximum allowable off-boresight angle.

To find the intervals that contain rise and set times without interpolating through every time step, the time steps in the coarse propagation for each satellite–station combination for which $f_R(t) \le 0$, $f_\phi(t) \le 0$, and $f_\theta(t) \ge 0$ are found. During these times, the satellite can access the ground station. Of these time steps, the times are found that are near the beginning interval of access by finding points that are more than one time step away from the previous point satisfying the constraints. Likewise, the times that are near the end of an interval are found by finding points that are more than one time step away from the next point satisfying the constraints. $f_R(t)$, $f_\phi(t)$, or $f_\theta(t)$, whichever is most restrictive at each point, is used for the quintic interpolation as described by Alfano to get the rise and set times [47]. The rise/set time occurs when the most restrictive function is equal to zero.

For each ground station, a matrix is constructed to describe the access to that station over time. The rows correspond to the sorted rise and set times, whereas the columns correspond to the satellites. The matrix is binary such that a one in the (i, j) place indicates that the jth satellite can access the ground station from the ith time until the $(i + 1)$th time. There is a corresponding vector of times, T_k, to match the rows of the matrix. An access array A is formed by concatenating the accesses for each station and a time matrix T. T_{ik} is the ith rise or set time for the kth station. A_{ijk} is one if the jth satellite can access the kth ground station between T_{ik} and $T_{(i+1)k}$. The length of each time step is calculated, $\Delta T_{ik} = T_{(i+1)k} - T_{ik}$. The access array and time matrix are used to calculate revisit metrics and in the resilience calculations outlined in the following section.

D. Resilience

This section discusses a method for formulating the problem of finding the combination of losses of assets most degrading to the constellation performance as an LP. The access array described in the previous section can be used in examining the performance of the degraded constellation. If the number of satellites is small and the number of predicted removals/failures is small, it is simple to check every combination of removals to determine the most damaging case. The columns of the access array that correspond to the removed satellites are removed, and the resilience metrics are calculated for the new array. However, because the problem grows combinatorially, evaluating all combinations directly for large problems quickly becomes infeasible. For example, Stenger considered 12-removal, 24-removal, and 36-removal cases for the 66-satellite Iridium constellation [17]. The smallest of these cases has 4.92×10^{12} combinations.

Mathematical programming is used to solve the problem of finding the worst combination of satellite removals, which can be formulated as a mixed integer linear program (MILP). The exact formulation will depend on the metric used in the optimization. In this analysis, the problem of finding the combination of removals that maximizes the longest gap in coverage seen by any of the ground stations (maximum revisit time over all points) is considered. The number of satellites in the nominal constellation is n_s, the number of removals is n_r, and the number of ground stations is n_g.

The decision variable $x_j \in \{0, 1\}\ \forall\ j = 1, 2, \ldots, n_s$ is a binary satellite inclusion variable that is one if the jth satellite is active and zero otherwise. To produce the correct number of removals, it is required that

$$\sum_{j=1}^{n_s} x_j = n_s - n_r \tag{19}$$

It is then necessary to determine how many satellites are available to each station at any given time. The access sum $\overline{A}_{ik}$ gives the number of satellites available to ground station k at its ith time step:

$$\overline{A}_{ik} = \sum_{j=1}^{n_s} A_{ijk} x_j \tag{20}$$

The next step is to calculate whether a sufficient number of assets is available for access at each period. n_c is the number of assets required to be in view of the ground station simultaneously for successful access. The calculation of this access requires the introduction of a new binary variable $Y_{ik} \in \{0, 1\}$. Y_{ik} is one if the required number of assets is accessible by station k at time i and zero otherwise. To force Y_{ik} to take the appropriate value, two more constraints are introduced. The second is a big-M constraint for which $M = n_s - n_c + 1$.

$$Y_{ik} \le \frac{\overline{A}_{ik}}{n_c} \qquad \forall\ i \in [1, \ldots, n_t - 1], k \in [1, \ldots, n_g] \tag{21}$$

$$MY_{ik} \ge \overline{A}_{ik} - n_c + 1 \quad \forall\ i \in [1, \ldots, n_t - 1], k \in [1, \ldots, n_g] \tag{22}$$

Equation (21) ensures that Y_{ik} is zero if insufficient satellites are available. Equation (22) ensures that Y_{ik} is one if at least n_c satellites are available.

The maximum revisit time of a ground station is the longest period for which that station is without coverage. The maximum revisit time over all points is the largest gap in coverage for any station in the scenario. The formulation begins with the definition of an accumulator variable $a_{ik} \in \mathbb{R}_{\ge 0}$. The accumulator variable counts the amount of time at each step since the end of the previous pass. During a pass and immediately after the pass ends, the accumulator should be zero. The constraints below are big-M constraints. To distinguish from the big-M value used in Eq. (21), the big-M value in these constraints will be referred to as M_2. The most conservative value for M_2 is the length of the scenario plus a small constant. However, using smaller values to aid convergence is encouraged if it is guaranteed that no gap will ever exceed the value chosen for M_2.

The constraints needed to force a_{ik} to take the appropriate value are slightly different for the first time step from that for the rest of the scenario. a_{1k} has the constraints

$$a_{1k} \ge \Delta T_{1k} - M_2 Y_{1k} \quad \forall\ k \in [1, \ldots, n_g] \tag{23}$$

$$a_{1k} \le \Delta T_{1k} + M_2 Y1k \quad \forall\ k \in [1, \ldots, n_g] \tag{24}$$

These constraints ensure that a_{1k} will be equal to the length of the first time step if there is no access when the scenario begins. The constraints for the rest of the time period are

$$a_{ik} \ge a_{(i-1)k} + \Delta T_{ik} - M_2 Y_{ik}\ \ \forall\ i \in [2, \ldots, n_t - 1], k \in [1, \ldots, n_g] \tag{25}$$

$$a_{ik} \le a_{(i-1)k} + \Delta T_{ik} + M_2 Y_{ik}\ \ \forall\ i \in [2, \ldots, n_t - 1], k \in [1, \ldots, n_g] \tag{26}$$

Likewise, these constraints ensure that a_{ik} will be equal to the previous accumulator value plus the time step if there is no access at the current time. Finally, a_{ik} must be zero if there is access at the current time, so

$$a_{ik} \le M_2(1 - Y_{ik}) \quad \forall\ i \in [1, \ldots, n_t - 1], k \in [1, \ldots, n_g] \tag{27}$$

The length of the largest gap is equal to the largest value of a_{ik}. To find this value, a variable $a_{\max} \in \mathbb{R}_{\ge 0}$ is introduced. Because the goal is to maximize $a_{\max}$, there must be an upper bound on $a_{\max}$ to prevent it growing unbounded. Therefore, it is required that $a_{\max}$ is less than or equal to exactly one of the values of a. To this end, additional binary variables $\delta_{ik} \in \mathbb{R}^{(n_t-1)\times n_g}$ are introduced. This formulation will drive $a_{\max}$ to the largest value of a and can be enforced with the constraints

$$a_{\max} \le a_{ik} + (1-\delta_{ik})M_2 \quad \forall\, i \in [1,\ldots,n_t-1], k \in [1,\ldots,n_g] \quad (28)$$

$$\sum_{i=1}^{n_t-1}\sum_{k=1}^{n_g}\delta_{ik} = 1 \quad (29)$$

The linear programming problem to determine the worst-case removals using maximum revisit time over all points is

$$\text{Minimize} - a_{\max}$$

with decision variables:

$$\begin{aligned}
x_j &\in \{0,1\} \quad \forall\, j \in [1,\ldots,n_s]\\
Y_{ik} &\in \{0,1\} \quad \forall\, i \in [1,\ldots,n_t], k \in [1,\ldots,n_g]\\
a_{ik} &\in \mathbb{R}_{\ge 0} \quad \forall\, i \in [1,\ldots,n_t-1], k \in [1,\ldots,n_g]\\
a_{\max} &\in \mathbb{R}_{\ge 0}\\
\delta_{ik} &\in \{0,1\} \quad \forall\, i \in [1,\ldots,n_t-1], k \in [1,\ldots,n_g]
\end{aligned}$$

subject to the constraints in Eqs. (19–29).

This formulation has a total of $(2n_t-1)\times n_g + n_s$ binary variables and $(n_t-1)\times n_g + 1$ continuous variables. State-of-the-art MILP solvers can handle hundreds of thousands of variables, but the ability of a solver to find a solution is dependent on more factors than simply the number of variables [48]. The distance between the relaxed and actual solutions, the number of constraints, and the ability of the solver to quickly find a feasible solution are only some of the factors that affect solve time. Some decision variables can be set a priori, reducing solve time. For example, any interval during which the nominal case did not have access to a sufficient number of assets will preclude the reduced case from having a sufficient number of assets, allowing the corresponding values of Y_{ik} to be set to zero. Similarly, if the nominal case had sufficient assets such that removing the maximum number of assets would not affect access during that period, the corresponding values of Y_{ik} can be set to one. Another method for decreasing runtime is to consider each ground station separately. Because the runtime of an MILP solver will increase in a nonpolynomial fashion with number of variables, it may be faster to run several small programs than one large one, depending on the solver overhead and the solve times for the two problem sizes. Meaning, one program with 100,000 variables will generally be slower than 100 programs with 1000 variables each. The results can then be combined by choosing the highest maximum revisit time from among all the ground stations.

The number of ground stations and time steps both have a more significant direct impact on the number of variables, though the number of times is a function of the number of satellites. It is possible to reduce the size of the problem by limiting the number of ground stations or the total duration of the scenario. Constellations with repeating ground tracks or whose formulations permit short analysis times will benefit most from this formulation due to the smaller number of variables required for such problems. The formulation is only beneficial in large combinatorial cases, as small cases can be handled more rapidly by full enumeration of all removal possibilities.

IV. Mars Scenario Description

To test the ability of the DISCO-Tech methodology to compare monolithic spacecraft constellations to disaggregated, heterogeneous constellations, a test case involving the design of a Mars-orbiting constellation was developed. The constellation's purpose is to provide baseline communications and position, navigation, and timing (PNT) capabilities in order to support a theoretical human settlement on Mars. Because of the difficulty of transporting equipment to the planet's surface, it is likely that much of Mars's infrastructure will be space based. Optimization was performed to find a constellation that could 1) provide voice communications for 5000 simultaneous users, 2) provide PNT capabilities globally, and 3) enable data transmission back to Earth with speeds of 1 Mbps. The ability to provide voice communications was quantified using a globally averaged maximum revisit time and a channel capacity constraint. Each voice transmission required a data rate of 9.6 kbps and a maximum bit error rate of 10^{-3}, which are standard requirements for satellite voice communications used by constellations such as Globalstar [20]. The ground segment of the communications link was modeled after current tactical radios, with a transmit power of 3.2 W and a gain of 1 dBi. The PNT requirement was considered to be satisfied if points on a defined grid across the globe had continuous coverage from at least four satellites with a data rate of 50 bps and a maximum bit error rate of 10^{-5}. It is assumed that the positioning satellites will have sufficient knowledge of their own positions from established ground stations or transmitters. The data transmission requirement was checked by examining the multistage link budget connecting a theoretical Mars high-powered ground station to the Deep Space Network on Earth in the worst-case scenario when Mars and Earth are separated by 2.5 AU, transmitting a signal at 8 GHz and 100 W with an antenna half power beamwidth (HPBW) of 0.36 deg. The frequency and gain parameters of the ground station were set to match those of the Mars Reconnaissance Orbiter [49]. The HPBW of satellite-based transmitters and receivers involved in the data transfer was also defined as 0.36 deg, though the power was set as a variable to be determined during the optimization. The maximum acceptable bit error rate was set at 10^{-7}. A single objective function was used that penalized solutions that did not meet the standards for coverage and communication established above but did not reward performance above the minimum requirements.

Four potential satellite types were considered for this analysis. DISCO-Tech's ability to dynamically increase or decrease the number of architectures under consideration was not leveraged for this problem. The first type, NAV, was a PNT-only satellite that transmitted at the low data rate of 50 bps. The second type, COMMS, was a communications satellite that had a variable number of channels available to permit multiple accesses. It was presumed that COMMS could transmit the necessary PNT signal with no additional equipment or power due to the low data rate. Also, COMMS could be assigned a deep space transmitter and receiver (DST/R), though it was not required. Both NAV and COMMS were assigned to Walker Delta constellations. The third type, MR, was a Mars-orbiting satellite hosting a deep space transmitter whose sole function was to transmit data to Earth or to a second relay constellation. It was assigned to a near-equatorial circular plane. A fourth type, SR, was added to consider the possibility of having lower-powered Mars-orbiting satellites transmit to relatively near Sun-orbiting satellites that could then transmit to one another to reach a satellite near Earth. An illustration of the potential transmission paths is shown in Fig. 4. The range of spacecraft and orbit parameters is shown in Table 1.

The simulation was run using the bicubic interpolation J4 propagator described in Ref. [25]. The simulation time period was initially set for 10 days, but it is checked over a longer period of time once the simulation is complete if the final solution contains satellites at different inclinations that would be subject to different perturbations. Potential launch vehicles were determined from previous and planned Mars missions and include the Polar Satellite Launch Vehicle (PSLV), the Space Launch System, and the Atlas V 541. The genetic algorithm used a mutation rate of 0.05 and a population size of 300. The top 1% of candidates were kept for the next generation, with the best candidate remaining unmutated. The top 70% were considered as potential parents. The optimization was permitted to run for up to 600 generations, with 50 generations of unchanged dominance considered sufficient to conclude the optimization. This scenario was originally presented in Ref. [50].

V. Mars Scenario Results

The simulation determined that the most cost-effective solution was to use a single type of satellite, a communications satellite augmented with an additional deep space transmitter and receiver. The resulting satellite and constellation had the parameters shown in Table 2, with visualization shown in Fig. 5. The satellite will have a mass of approximately 120 kg. The estimated costs for the constellation, in

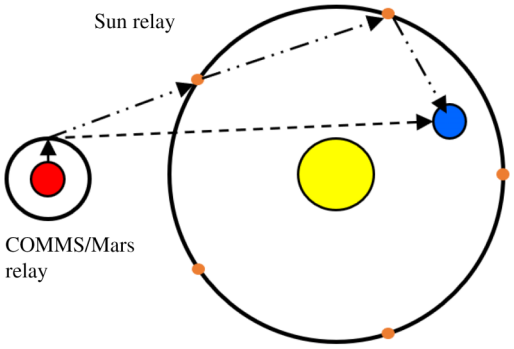

Fig. 4 Potential data relay paths.

Table 2 Mars solution properties

Property	Value
Communications frequency (GHz)	0.2
Communications transmit power (W)	6.5
Communications half power beamwidth (deg)	26
Communications number of channels	173
Semimajor axis (km)	9818
Inclination (deg)	85.2
Satellites per plane	9
Number of planes	5
Walker phasing parameter	1
Deep space transmit power (W)	29.3

2020 dollars, are $1.5 billion for development, $32 million for the first flight unit, $1.1 billion for all satellites, and $266 million for 15 PSLVs, giving a total mission cost of $2.9 billion.

The constellation provides continuous fourfold coverage over the entire planet. The maximum geometric dilution of precision of the constellation ranges between 1.2 and 2.1 for various latitudes. The voice communications have an uplink bit error rate of 6.9×10^{-5} and a downlink bit error rate of 6.7×10^{-5}. The link budget for the downlink is shown in the Appendix. The bit error rate for the PNT data is insignificant due to the low data rate. The bit error rate for data transmission to Earth is 8.3×10^{-8}.

The semimajor axis of the orbit is 9818 km, which is close to the orbit of Phobos. Phobos's orbit has a periapsis radius of 9234 km and an apoapsis radius of 9518 km. Because the distance between the orbits and Phobos can be as small as 300 km, an additional simulation was performed to determine whether a collision was possible. Ten thousand sets of satellite orbital elements with random RAANs and initial true anomalies were generated. A force model that includes a fourth-order gravitational model of Mars and a point mass model of Phobos as a third body was developed. At a distance of 300 km, the acceleration due to Phobos is on the order of 10^{-5} m/s^2. Satellites were propagated using the generated orbital elements (OEs) and this force model for a simulation time of 3 years. During this time period, the closest approach for any satellite to the moon was 258 km. The average closest approach was 296 km, and the standard deviation for the closest approach was 14 km. As Phobos's radius is only 11 km, there appears to be sufficient separation that collision is not a concern. This result could be further validated using a higher-fidelity force model, or the optimization could be repeated after restricting permissible values of the semimajor axis to exclude regions near the moon.

The constellation tool performed as expected, with the optimization undergoing 239 generations before 50 generations of continuous dominance were achieved. Ultimately, a single satellite type was the most viable due to development and launch costs, which could have eliminated the two relay satellite types. The number of communications satellites needed made the additional PNT satellites unnecessary. If a satellite were made with COTS components and the cost modeled accordingly, it is possible that a multiple satellite solution would become preferable. Furthermore, if the target area of the communications constellation were reduced to the equatorial region, it is likely that the lower-cost PNT satellites would be a superior choice to provide the remaining coverage. To ensure that additional satellite types were not prematurely excluded, additional runs can be performed both of the same simulation and of simulations that force the inclusion of additional satellite types. Regardless, this scenario demonstrated the capability of DISCO-Tech to compare the performance of heterogeneous and homogeneous constellations. The fact that the optimal solution was a homogeneous constellation highlights the need to avoid prematurely eliminating architecture options due to a preconceived notion of what the best solution may be.

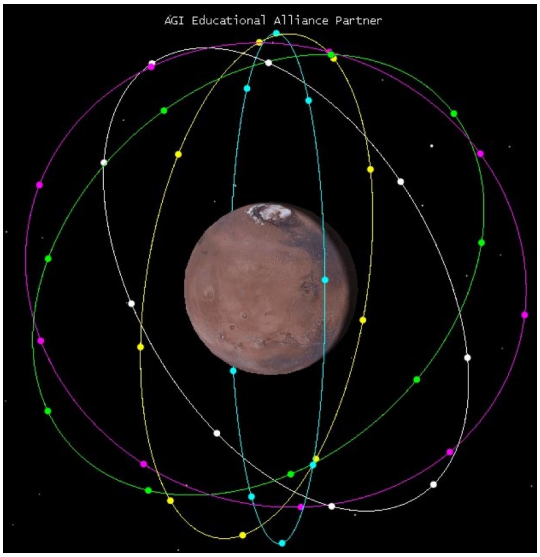

Fig. 5 Visualization of final constellation.

Table 1 Mars optimization ranges

Property	NAV	COMMS	MR	SR
TX frequency (GHz)	[0.2, 0.4, 1.5, 2.5, 5.9, 7.9]	[0.2, 0.4, 1.5, 2.5, 5.9, 7.9]	8.0	8.0
TX power (W)	0.1–50	0.1–1000	10–500	10–500
HPBW (deg)	10–180	10–180	0.36	0.36
Channels	1	1–1000	1	1
a (km)	3,596–21,396	3,596–21,396	3,596–21,396	$(1.496–2.274) \times 10^8$
i (deg)	2–90	2–90	2	0
SatsPP	1–20	1–20	1–20	1–10
No. of planes	1–20	1–20	1	1
Central body	Mars	Mars	Mars	Sun
Optional payloads	— —	DST/R (10-500 W)	— —	— —

HPBW, half power beamwidth (SatsPP = satellites per plane, TX = transmit).

VI. Rideshare Scenario Description

One benefit of both nanosatellites and rideshare launches is the ability to use them on short notice. This feature is especially beneficial in the event of an emergency, when there is insufficient time to build and deploy a traditional satellite constellation. To simulate such a scenario, consider the case of fire detection over California. The goal is to deploy a constellation of nanosatellites constructed of COTS parts using rideshare opportunities in a timely manner. The nanosatellites are identical and have the following subsystems:

1) Propulsion: 2U propulsion module with a thrust of 1.25 N, a specific impulse of 235 s, and a propellant mass of 1.4 kg[**]

2) Antenna: deployable helical antenna

3) Transmitter/receiver: VHF downlink/UHF uplink full duplex transceiver

4) Battery: high-energy-density battery array

5) Electrical power subsystem: CubeSat power supply

6) Solar panels: CubeSat solar panels

7) Attitude control system: CubeSat three-axis reaction wheels and magnetorquers

8) Imager: multispectral imager with a ground sample distance of 9.6 m at 500 km[††]

With the exception of the propulsion system and the imager, the components listed above serve only to estimate the cost and mass required for the satellite and do not represent a finalized design. The propulsion system dictates the maneuvers that can be performed by the satellite, whereas the imager dictates the image resolution, limiting the maximum altitude of the satellites.

A set of rideshare options was simulated by taking the two line elements (TLEs) of satellites launched over a 30-day period. This sampling is meant to be an example set of launches and is not indicative of the launches that would be available for an actual mission. The results will vary based on the particular set of launches available. The orbital elements corresponding to the TLEs are shown in Table 3, where each row represents a different launch with the angles are in degrees and the semimajor axis in kilometers. Orbital elements are presented with respect to the Earth-centered inertial (ECI) frame.

The optimization selects a set of launches, assigns satellites to each selected launch, and sets a reconfiguration for each launch by setting the change in orbital elements. The satellites' orbital elements will be the orbital elements of the launch plus the change in orbital elements. The satellites will be evenly distributed in true anomaly around the orbit. The reachability methodology described in the previous section is used to check if the initial orbit and final orbits produced by the optimizer are compatible (reachable within 10 orbits using the available propellant and thrust). A segment of the genome produced by the genetic algorithm would have the form $\boldsymbol{x}_i = [$launch assignment, number of satellites, Δa, Δe, Δi, $\Delta\omega$, $\Delta\Omega$, $\Delta\theta]$. The genome is permitted to have between 1 and 20 segments. It is possible that multiple planes of satellites may be deployed from a single launch by assigning multiple orbital element changes to one launch. In a simulation of a real-life scenario, it would be beneficial to introduce a constraint ensuring that the mass capacity for rideshare of a vehicle is not exceeded. The total number of satellites launched is not to exceed 50.

Because the goal of the scenario is to maximize coverage over the state of California, a set of points evenly spaced with 100 miles between them was generated within the state. A minimum elevation limit for access of 5 deg was imposed. A maximum ground sample distance (GSD) of 25 m is also required for access. The satellites are assumed to be able to slew sufficiently to cover the area of interest, so no constraint is imposed on the off-boresight angle of the satellite.

The access provided by a given solution is evaluated using two metrics: the average time average gap (TAG) of the ground points and the maximum revisit time over all points. The TAG of a ground point is defined as [51]

Table 3 Rideshare orbital elements, ECI

Launch	a	e	i	ω	Ω
1	6,823	0.0018	92.9	118.3	253.5
2	6,823	0.0018	92.9	118.6	253.5
3	6,823	0.0017	92.9	124.2	253.5
4	6,823	0.0018	92.9	124.6	253.5
5	6,966	0.0014	97.9	153.2	158.3
6	6,966	0.0014	97.9	151.1	158.3
7	28,241	0.0117	55.0	176.3	156.9
8	28,243	0.0116	55.0	176.4	156.9
9	7,090	0.0091	98.6	337.4	340.2
10	15,700	0.5808	55.0	172.5	153.7
11	15,531	0.5723	26.9	195.9	240.4
12	7,161	0.0011	98.6	165.3	339.7
13	6,673	0.0021	51.6	340.3	237.9
14	6,837	0.0019	91.9	59.6	251.1
15	6,975	0.0032	97.7	175.0	158.0
16	6,784	0.0008	51.6	35.9	237.1
17	42,133	0.0010	0.0	96.4	95.9
18	28,820	0.0089	54.9	4.6	156.8

$$\text{TAG} = \frac{\sum^{\text{gaps}} (\text{Gap Duration})^2}{\text{Coverage Interval}} \tag{30}$$

TAG provides the average time until next coverage for a given ground point when starting from an arbitrary time in the scenario. The maximum revisit time over all points calculates the longest time that each point is without coverage and then takes the largest of these values. The total number of satellites is minimized in order to survey the entire solution space and to determine the coverage possible at varying asset levels.

Because of the relatively high failure rate of nanosatellites, it is necessary to consider the possibility that some of the satellites may fail prematurely. The impact of this possibility is measured by determining the worst-case maximum revisit time over all points when 20% of the satellites are removed from the scenario. The linear programming approach discussed in the "Resilience" subsection of the previous section is applied in order to obtain this worst-case objective value. The optimization problem therefore has four objectives: minimize average TAG, minimize maximum revisit time over all points, minimize degraded maximum revisit time over all points, and minimize number of satellites.

A scenario time of 30 days is used when calculating the nominal objectives. The degraded analysis uses a 10-day scenario time to limit the size of the linear programming problem. The simulation is run until 10 successive generations produce no improvement in the archive. A new population is then generated using the archive and randomly generated members, as described in Ref. [27]. An initial population of 200 candidates is used, with the population being scaled each run to be four times the archive size. This process is repeated for 10 runs. For comparison purposes, optimization is performed on a Walker delta constellation with up to 50 satellites and up to 20 planes. The Walker formulation does not undergo reconfiguration. It seeks to minimize the total number of planes in addition to the objectives stated for the rideshare scenario. This scenario was originally presented in Ref. [52].

VII. Rideshare Scenario Results

The rideshare simulation produced a nondominated frontier with 31 results, shown in Fig. 6. The TAG of the nondominated solutions ranges from 52 minutes for the larger constellations to 11.2 h for a single satellite. The maximum revisit time over all points takes values between 3.8 and 12.4 h. The degraded maximum revisit time over all points takes values between 5.0 and 11.6 h, discounting the single-satellite case. After the 10th satellite, additional satellites produce diminishing returns. Indeed, the objective values change very slightly between 20 and 35 satellites. Figure 7 colors the nondominated frontier by the number of orbital planes (and therefore launches) used by each solution. The theoretical FireSat-II example in Ref. [18]

**http://www.rocket.com/files/aerojet/documents/CubeSat/MPS-130%20data%20sheet%20crop.pdf.

††http://41.185.8.177/~cubespac/ClientDownloads/CubeADCS_3Axis_Specsheet_V1.1.pdf.

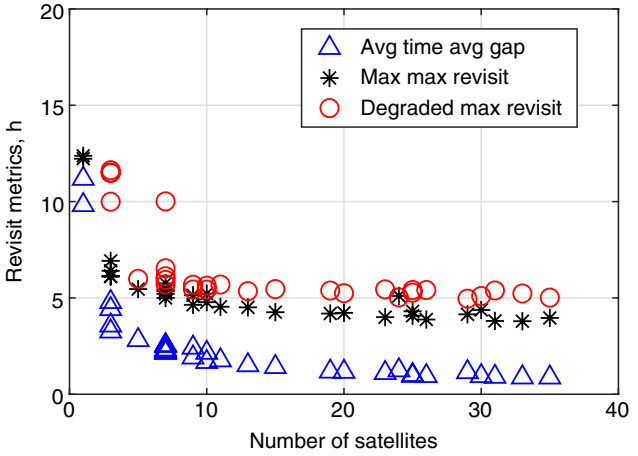

Fig. 6 Nondominated frontier for rideshare-launched constellation.

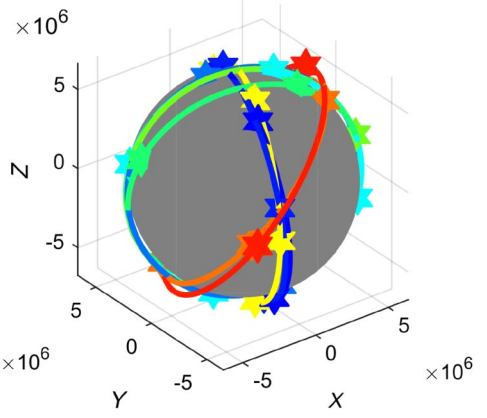

Fig. 8 Example constellation of 30 satellites.

requires a revisit time of 8 h to identify nascent forest fires. The imaging capability provided by the rideshare constellations is sufficient to meet these requirements. The rideshare constellation coverage performance is inferior to proposed constellation designs such as the FUEGO program, which achieves 25-minute revisit times using dedicated launches [53].

An example rideshare constellation using 30 satellites is shown in Fig. 8. The constellation consists of two sets of near-polar orbits spaced about 90 deg apart in RAAN, plus a pair of orbits near 50 deg in inclination. During the 30-day simulation time, the polar orbits maintain similar relative positions, but the relative position of the 50 deg orbits with respect to the polar orbits vary.

The stagnation of the values with increasing numbers of satellites highlights the critical flaw in rideshare constellations. Because the initial launches are fixed in such a way that may not be beneficial to the rideshare mission, the resulting constellation can have large gaps in coverage when the rideshare orbits do not overlap in a fortuitous manner. The ability to maneuver the satellites helps to mitigate the problem, but the high propellant cost to enact a change in orbital plane impedes the constellation's ability to achieve the uniform formation often used in constellation design.

There are two ways to increase the performance of the rideshare constellation. The first is to have a greater number of rideshare opportunities available. By permitting the satellites to be launched over a longer time period, more rideshares become available, increasing available orbit diversity. However, spreading the launch of the constellation over a longer period of time decreases the overall life of the constellation because the time from when the constellation is fully populated to when the first satellite reaches the end of its life is decreased. The other method for increasing constellation performance and spacing between orbits is to increase the maneuvering capability of the satellites. Maneuvering can be improved by either increasing the amount of propellant onboard the satellites or by using a low-thrust, high-I_{sp} electric propulsion system. The latter option increases the overall maneuverability, but requires more time for the constellation to reach its final configuration.

The performances of the rideshare constellations are compared with Walker constellations optimized using the genetic algorithm. The nondominated frontier for the Walker case is shown in Fig. 9. As expected, the Walker constellations offer superior performance over the rideshare constellations. A Walker constellation of 4 satellites has comparable performance to a rideshare constellation of 15–20 satellites. Furthermore, satellites can be added to the Walker constellation to improve coverage until continuous coverage is reached, whereas the rideshare constellation has unfillable gaps due to the relative placement of the rideshare orbits. However, the cost of launching four satellites on dedicated rides is significantly greater than the cost of the additional satellites needed for the rideshare constellation. The cost for the components listed in the previous section is $283K for everything except the propulsion system, which is still in development and does not have a published price. If the total cost is approximately $400K with the propulsion system, the satellite cost would be $6M for the rideshare constellation and $1.6M for the Walker constellation. Neither price includes the cost of testing or software development. The Walker constellation would require 2–4 launches to LEO, a cost of $36.8M–73.6M using Pegasus XL rockets [18]. Conversely, with a $30K per kilogram rideshare launch cost and a spacecraft weighing about 10 kg, the rideshare launch cost is only $4.5M. Therefore, if the performance limitations of the rideshare constellation are acceptable, a constellation can be developed for about a quarter of the cost of a traditional Walker constellation. Fires in the state of California cause billions of dollars in damage each year, so the low cost of a fire detection constellation has the potential to pay for itself many times over.

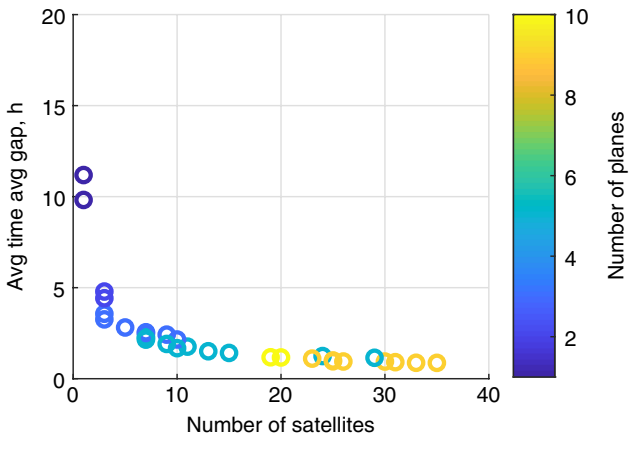

Fig. 7 Average time average gap for rideshare-launched constellation.

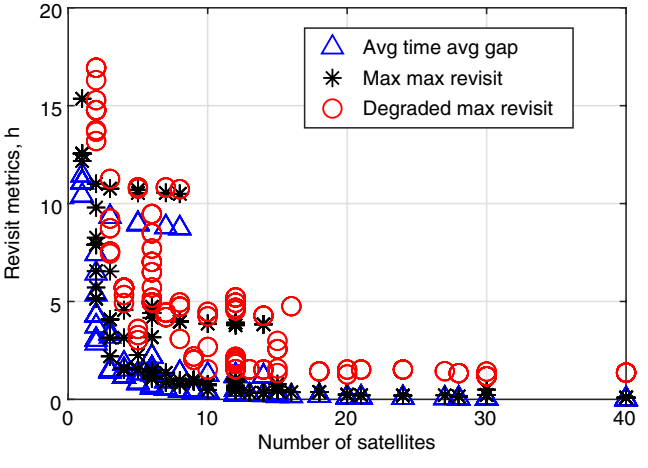

Fig. 9 Nondominated frontier for Walker constellation.

VIII. Conclusions

This paper outlines a methodology for designing and analyzing nontraditional satellite constellations, including disaggregated and rideshare constellations. Particular emphasis is given to new methodologies for reachability and resilience analyses for constellations of nanosatellites. These methods leverage linear programming techniques and offer savings in computation time over other methods. A validation case of designing a Mars-orbiting navigation and communications constellation is discussed, with the result being that traditional, homogeneous constellations are more appropriate for this scenario. The methodology is also used to analyze the ability of a constellation built using only rideshare opportunities to provide coverage over California to perform fire detection. An average time average gap of less than 1 h is achievable, as is a maximum revisit time over all points of less than 4 h. The rideshare performance is compared with the performance of a Walker constellation. Although the Walker constellation can achieve arbitrary levels of coverage through the addition of further satellites, rideshare constellations are capable of meeting the capabilities of small Walker constellations at greatly reduced cost. Future work will extend the DISCO-Tech methodology to other nontraditional constellation types, such as multidomain and hosted payload constellations. It will also examine options for improved optimization of dynamic constellations and compare performance to that of other constellation design tools.

Appendix: Link Budget

The link budget for the voice communications satellites is shown in Table A1.

Table A1 Voice communications link budget

Parameter	dB value	Supporting value
Downlink frequency		200 MHz
Transmit power	8.13 dBW	6.5 W
Peak transmit antenna gain	14.45 dBi	
Transmit FOV loss	−2.78 dB	
Transmit line loss	−0.75 dB	
EIRP	19.09 dBW	
Number of channels		173
EIRP per channel	**−3.33 dBW**	
Space loss	−155.36 dB	
Atmospheric loss	0 dB	
Propagation and polarization loss	−0.75 dB	
Losses	**−157.95 dB**	
Receiver gain	**1.00 dBi**	
Boltzmann's constant, k		1.38×10^{-23} J/K
$1/k$	228.60 dBK/J	7.2×10^{22} K/J
Noise temperature, T		201.76 K
$1/T$	−23.05 dB/K	4.95×10^{-3} 1/K
Data rate per channel, R		9.6 kbps
$1/R$	−39.82 dB/Hz	1.04×10^{-4} s/bit
1/(kRT)	**165.73 dB/Hz/J**	
E_b/N_0	**7.29 dB**	
Required E_b/N_0	**6.67 dB**	
Link margin	**0.62 dB**	

FOV = field of view, EIRP = effective isotropic radiated power. Bolded terms are components of link equation: $E_b/N_0 = \text{EIRP per channel} + \text{Losses} + \text{Receiver gain} + 1/(\text{kRT})$. Link margin = E_b/N_0 − Required Eb_b/N_0.

Acknowledgments

This material is based upon work supported by the National Science Foundation Graduate Research Fellowship Program under Grant No. DGE-1651272. Any opinions, findings, and conclusions or recommendations expressed in this material are those of the author(s) and do not necessarily reflect the views of the National Science Foundation. Support for this work was also provided by the Virginia Tech Institute for Critical Technology and Applied Science, the Ted and Karyn Hume Center for National Security and Technology, and the Virginia Space Grant Consortium.

References

[1] Sweeting, M., "Modern Small Satellites-Changing the Economics of Space," *Proceedings of the IEEE*, Vol. 106, No. 3, 2018, pp. 343–361. https://doi.org/10.1109/PROC.5

[2] "Smallsats by the Numbers 2018," Bryce Space and Technology, Alexandria, VA, Tech. Rept. 43, 2019.

[3] Barnhart, D. J., Vladimirova, T., and Sweeting, M. N., "Very-Small-Satellite Design for Distributed Space Missions," *Journal of Spacecraft and Rockets*, Vol. 44, No. 6, 2007, pp. 1294–1306. https://doi.org/10.2514/1.28678

[4] Helvajian, H., and Janson, S. W., *Small Satellites: Past, Present, and Future*, Aerospace Press, El Segundo, CA, 2008, pp. 151–174, 711–810. https://doi.org/10.2514/4.989223

[5] Janson, S., "25 Years of Small Satellites," *Proceedings of the 25th Annual AIAA/USU Conference on Small Satellites (SSC11-III-1)*, AIAA, Reston, VA, 2011.

[6] Bedingfield, K. L., Leach, R. D., and Alexander, M. B., "Spacecraft System Failures and Anomalies Attributed to the Natural Space Environment," NASA TR 1390, 1996.

[7] Pawlikowski, E., Loverro, D., and Cristler, T., "Space: Disruptive Challenges, New Opportunities, and New Strategies," *Strategic Studies Quarterly*, Vol. 6, No. 1, 2012, pp. 27–54.

[8] "Resiliency and Disaggregated Space Architectures," Air Force Space Command Tech. Rept. AFD-130821-034, 2013.

[9] Thompson, R. E., Colombi, J. M., Black, J., and Ayres, B. J., "Model-Based Conceptual Design Optimization Methods: Disaggregated Weather System Follow-On," *Journal of Spacecraft and Rockets*, Vol. 52, No. 4, 2015, pp. 1021–1037. https://doi.org/10.2514/1.A33135

[10] Hastings, D. E., Tour, P. A. L., and Giri, D. K., "The Architectural Concept of Disaggregation of Space Systems: Application to Weather Satellites," *Journal of Spacecraft and Rockets*, Vol. 56, No. 5, 2019, pp. 1492–1507. https://doi.org/10.2514/1.A34353

[11] Lam, J. F., Tour, P. L., and Kim, J., "Architecting Disaggregated Space Weather Solutions Using Nanosatellites," *AIAA SPACE 2013 Conference and Exposition*, AIAA Paper 2013-5322, 2013. https://doi.org/10.2514/6.2013-5322

[12] Thompson, R. E., Colombi, J. M., Black, J., and Ayres, B. J., "Disaggregated Space System Concept Optimization: Model-Based Conceptual Design Methods," *Systems Engineering*, Vol. 18, No. 6, 2015, pp. 549–567. https://doi.org/10.1002/sys.21310

[13] Colombi, J. M., Stern, J. L., Wachtel, S. T., Meyer, D. W., and Cobb, R. G., "Multi-Objective Parallel Optimization of Geosynchronous Space Situational Awareness Architectures," *Journal of Spacecraft and Rockets*, Vol. 55, No. 6, 2018, pp. 1453–1465. https://doi.org/10.2514/1.A34043

[14] Venturini, C. C., "Improving Mission Success of CubeSats," The Aerospace Corp. Tech. Rept. TOR-2017-01689, 2017.

[15] Peng, Z., and Kohani, S., "The Performance of the Constellations Satellites Based on Reliability," *Journal of Space Safety Engineering*, Vol. 4, No. 2, 2017, pp. 112–116. https://doi.org/10.1016/j.jsse.2017.07.003

[16] Hastings, D. E., and Tour, P. A. L., "An Economic Analysis of Disaggregation of Space Assets: Application to GPS," *Acta Astronautica*, Vol. 134, May 2017, pp. 244–264. https://doi.org/10.1016/j.actaastro.2017.02.008

[17] Stenger, D. K., "Survivability Analysis of the Iridium Low Earth Orbit Satellite Network," Master's Thesis, Air Force Inst. of Technology, Wright–Patterson AFB, OH, 1996.

[18] Wertz, J., Everett, D., and Puschell, J., *Space Mission Engineering: The New SMAD*, 1st ed., Space Technology Library, Microcosm Press, Hawthorne, CA, pp. 298, 299, 316, 486.

[19] Berk, J., Straub, J., and Whalen, D., "The Open Prototype for Educational NanoSats: Fixing the Other Side of the Small Satellite Cost Equation," *2013 IEEE Aerospace Conference*, IEEE, New York, 2013, pp. 1–16. https://doi.org/10.1109/AERO.2013.6497393

[20] Larson, W. J., and Wertz, J. R. (eds.), *Space Mission Analysis and Design*, 3rd ed., Space Technology Library, Microcosm Press and Kluwer Academic Publishers, El Segundo, CA, pp. 533–586. https://doi.org/10.1007/978-94-011-2692-2

[21] "ELaNa XII CubeSat Launch on NROL-55 Mission," NASA Tech. Rept. NF-2015-10-594-HQ, 2015.

[22] Ellis, A., Mercury, M., and Brown, S., "Global Coverage from Ad-Hoc Constellations in Rideshare Orbits," *Proceedings of the 26th Annual*

AIAA/USU Conference on Small Satellites (SSC12-IV-3), AIAA, Reston, VA, 2012.

[23] Gangestad, J. W., Wilson, J. R., Gates, K. L., and Langer, J. V., "Rideshare-Initiated Constellations: Future CubeSat Architectures with the Current Launch Manifest," *Proceedings of the 31st Space Symposium*, Space Foundation, Colorado Springs, CO, 2015, pp. 1–18.

[24] Colombi, J. M., Buckle, L. D., Black, J. T., and Nurre, S. G., "Optimal Launch Manifesting for Heterogeneous Disaggregated Satellite Constellations," *Journal of Spacecraft and Rockets*, Vol. 54, No. 3, 2017, pp. 582–591. https://doi.org/10.2514/1.A33796

[25] Mott, K. E., and Black, J. T., "Model-Based Heterogeneous Optimal Space Constellation Design," *2018 21st International Conference on Information Fusion (FUSION)*, Inst. of Electrical and Electronics Engineers, New York, 2018, pp. 602–609. https://doi.org/10.23919/ICIF.2018.8455222

[26] Ferringer, M. P., Spencer, D. B., and Reed, P., "Many-Objective Reconfiguration of Operational Satellite Constellations with the Large-Cluster Epsilon Non-Dominated Sorting Genetic Algorithm-II," *2009 IEEE Congress on Evolutionary Computation*, Inst. of Electrical and Electronics Engineers, New York, 2009, pp. 340–349. https://doi.org/10.1109/CEC.2009.4982967

[27] Hadka, D., and Reed, P., "Borg: An Auto-Adaptive Many-Objective Evolutionary Computing Framework," *Evolutionary Computing*, Vol. 21, No. 2, 2013, pp. 231–259. https://doi.org/10.1162/EVCO_a_00075

[28] Ferringer, M. P., Clifton, R. S., and Thompson, T. G., "Efficient and Accurate Evolutionary Multi-Objective Optimization Paradigms for Satellite Constellation Design," *Journal of Spacecraft and Rockets*, Vol. 44, No. 3, 2007, pp. 682–691. https://doi.org/10.2514/1.26747

[29] Pegher, D. J., and Parish, J. A., "Optimizing Coverage and Revisit Time in Sparse Military Satellite Constellations: A Comparison of Traditional Approaches and Genetic Algorithms," Master's Thesis, Naval Postgraduate School, Monterey, CA, 2004.

[30] Lee, H. W., Jakob, P. C., Shimizu, S., and Yoshikawa, S., "Optimization of Satellite Constellation Deployment Strategy Considering Uncertain Areas of Interest," *Acta Astronautica*, Vol. 153, Dec. 2018, pp. 213–228. https://doi.org/10.1016/j.actaastro.2018.03.054

[31] Legge, R. S., Jr., and Miller, D. W., "Optimization and Valuation of Reconfigurable Satellite Constellations Under Uncertainty," Ph.D. Thesis, Massachusetts Inst. of Technology, Cambridge, MA, 2014.

[32] Appel, L., Guelman, M., and Mishne, D., "Optimization of Satellite Constellation Reconfiguration Maneuvers," *Acta Astronautica*, Vol. 99, June 2014, pp. 166–174. https://doi.org/10.1016/j.actaastro.2014.02.016

[33] Fakoor, M., Bakhtiari, M., and Soleymani, M., "Optimal Design of the Satellite Constellation Arrangement Reconfiguration Process," *Advances in Space Research*, Vol. 58, No. 3, 2016, pp. 372–386. https://doi.org/10.1016/j.asr.2016.04.031

[34] Xue, D., Li, J., Baoyin, H., and Jiang, F., "Reachable Domain for Spacecraft with a Single Impulse," *Journal of Guidance, Control, and Dynamics*, Vol. 33, No. 3, 2010, pp. 934–942. https://doi.org/10.2514/1.43963

[35] Holzinger, M. J., Scheeres, D. J., and Erwin, R. S., "On-Orbit Operational Range Computation Using Gauss's Variational Equations with J2 Perturbations," *Journal of Guidance, Control, and Dynamics*, Vol. 37, No. 2, 2014, pp. 608–622. https://doi.org/10.2514/1.53861

[36] HomChaudhuri, B., Oishi, M., Shubert, M., Baldwin, M., and Erwin, R. S., "Computing Reach-Avoid Sets for Space Vehicle Docking Under Continuous Thrust," *2016 IEEE 55th Conference on Decision and Control*, Inst. of Electrical and Electronics Engineers, New York, 2016, pp. 3312–3318. https://doi.org/10.1109/CDC.2016.7798767

[37] Zagaris, C., and Romano, M., "Applied Reachability Analysis for Spacecraft Rendezvous and Docking with a Tumbling Object," *2018 Space Flight Mechanics Meeting*, AIAA Paper 2018-2220, 2018. https://doi.org/10.2514/6.2018-2220

[38] Breger, L., and How, J. P., "Gauss's Variational Equation-Based Dynamics and Control for Formation Flying Spacecraft," *Journal of Guidance, Control, and Dynamics*, Vol. 30, No. 2, 2007, pp. 437–448. https://doi.org/10.2514/1.22649

[39] Walker, M. J. H., Ireland, B., and Owens, J., "A Set of Modified Equinoctial Orbital Elements," *Celestial Mechanics*, Vol. 36, No. 4, 1985, pp. 409–419. https://doi.org/10.1007/BF01227493

[40] Walker, M. J. H., "Errata, A Set of Modified Equinoctial Orbital Elements," *Celestial Mechanics*, Vol. 38, No. 4, 1986, pp. 391–392. https://doi.org/10.1007/BF01238929

[41] Marcuccio, S., Pergola, P., Gregucci, S., and Andrenucci, M., "Low-Thrust Propulsion Systems for Small Satellites," *Proceedings of the 66th International Astronautical Congress*, Paper IAC-15.C4.6.7, International Astronautical Federation, Jerusalem, 2015.

[42] Thomas, D., Mott, K., Tetreault, K., Nastasi, K. M., Elliott, I., Scheible, R., Ohriner, E., and Black, J., "Real-Time On-Board Estimation and Optimal Control of Autonomous Micro-Satellite Proximity Operations," *55th AIAA Aerospace Sciences Meeting, AIAA SciTech Forum*, AIAA Paper 2017-0398, 2017. https://doi.org/10.2514/6.2017-0398

[43] Ebinuma, T., Bishop, R. H., and Lightsey, E. G., "Integrated Hardware Investigations of Precision Spacecraft Rendezvous Using the Global Positioning System," *Journal of Guidance, Control, and Dynamics*, Vol. 26, No. 3, 2003, pp. 425–433. https://doi.org/10.2514/2.5080

[44] Singla, P., Subbarao, K., and Junkins, J. L., "Adaptive Output Feedback Control for Spacecraft Rendezvous and Docking Under Measurement Uncertainty," *Journal of Guidance, Control, and Dynamics*, Vol. 29, No. 4, 2006, pp. 892–902. https://doi.org/10.2514/1.17498

[45] Wiesel, W. E., *Spaceflight Dynamics*, 3rd ed., CreateSpace, Scotts Valley, CA, 2010, pp. 97–100.

[46] Vallado, D. A., *Fundamentals of Astrodynamics and Applications*, 4th ed., Microcosm Press, Hawthorne, CA, 2013, pp. 609–654, Chap. General Perturbation Techniques.

[47] Alfano, S., "Rapid Generation of Site/Satellite Timetables," *Journal of Spacecraft and Rockets*, Vol. 30, No. 6, 1993, pp. 760–764. https://doi.org/10.2514/3.26383

[48] Koch, T., Achterberg, T., Andersen, E., Bastert, O., Berthold, T., Bixby, R. E., Danna, E., Gamrath, G., Gleixner, A. M., Heinz, S., Lodi, A., Mittelmann, H., Ralphs, T., Salvagnin, D., Steffy, D. E., and Wolter, K., "MIPLIB 2010," *Mathematical Programming Computation*, Vol. 3, No. 2, 2011, pp. 103–163. https://doi.org/10.1007/s12532-011-0025-9

[49] Taylor, J. (ed.), *Deep Space Communications*, 1st ed., JPL Deep-Space Communications and Navigation Series, Wiley, Hoboken, NJ, 2016, pp. 201–259, Chap. Mars Reconnaissance Orbiter. https://doi.org/10.1002/9781119169079.ch6

[50] Mott, K. E., and Black, J. T., "Heterogeneous Constellation Design Methodology Applied to a Mars-Orbiting Communications and Positioning Constellation," *AAS/AIAA Astrodynamics Conference, 2017*, Advances in the Astronautical Sciences Series, Vol. 162, Univelt, Stevenson, WA, 2017, pp. 2383–2396.

[51] "Measuring the Average Length of the Coverage Gap," 2018, http://help.agi.com/stk/index.htm#cov/fom-10.htm.

[52] Mott, K. E., and Black, J. T., "Design of a Resilient Rideshare-Based Small Satellite Constellation Using a Genetic Algorithm," *Advances in the Astronautical Sciences AAS/AIAA Space Flight Mechanics 2019*, Vol. 168, Univelt, Stevenson, WA, 2019, pp. 2399–2418.

[53] Escorial, D., Tourne, I. F., Reina, F. J., and Gonzalo, J., "FUEGO: A Dedicated Constellation of Small Satellites to Detect and Monitor Forest Fires," *Acta Astronautica*, Vol. 52, Nos. 9–12, 2003, pp. 765–775. https://doi.org/10.1016/S0094-5765(03)00052-3

Y. Xu
Associate Editor